Environmental Science and Pollution Research (2024) 31:50983–50999
https://doi.org/10.1007/s11356-024-34552-8

RESEARCH ARTICLE

Enhancing visible-light-driven photocatalysis: unveiling the remarkable potential of H_2O_2-assisted MOF/COF hybrid material for organic pollutant degradation

Amila Kasun Abeysinghe[1] · Yen-Ping Peng[1] · Po-Jung Huang[2] · Ku-Fan Chen[3] · Chia-Hung Chen[1] · Wu-Xing Chen[1] · Fang-Yu Liang[1] · Po-Yen Chien[1]

Received: 9 January 2024 / Accepted: 24 July 2024 / Published online: 6 August 2024

Abstract

In this study, we synthesized MOF/COF hybrid material (NH_2-MOF-5/MCOF) by integrating NH_2-MOF-5 (Zn) with a melamine-based COF (MCOF) to target the photocatalytic degradation of methylene blue (MB) dye. Characterization using SEM, XRD, XPS, FT-IR, and UV-DRS confirmed the synthesized MOF/COF hybrid's exceptional photocatalytic performance under visible light. The addition of H_2O_2 significantly enhanced the photocatalytic degradation, achieving removal rates of 90%, 92%, and 57% for 11.75 mg L^{-1}, 30 mg L^{-1}, and 83 mg L^{-1} of MB, respectively. Kinetic studies revealed first-order kinetics, with a rate constant nearly 3.5 times higher with added H_2O_2. We proposed a comprehensive photocatalytic mechanism elucidated through energy band structure analysis and scavenger tests. Our findings revealed the formation of a heterojunction between NH_2-MOF-5 and MCOF, which mitigates electron–hole recombination, with •OH identified as the principal species governing methylene blue degradation. Moreover, the NH_2-MOF-5/MCOF hybrid displayed excellent reusability and chemical stability over six cycles. Notably, this H_2O_2-assisted hybrid material demonstrated the removal of 99% of ibuprofen, a pharmaceutical drug, showcasing its broad applicability in removing organic contaminants in aqueous solutions, thereby holding great promise for wastewater treatment.

Keywords Energy band · Ibuprofen · Scavenger test · Heterojunction photocatalyst · Organic contaminants · Wastewater treatment

Introduction

Methylene blue (MB), a cationic dye belonging to the thiazine class, finds widespread application across various industrial sectors due to its vibrant color and versatile properties (Slama et al. 2021). In sectors such as textiles, leather, and printing, MB is commonly utilized for dyeing cotton, wool, and silk fabrics, as well as in the production of photographic materials and medical diagnostics (Khan et al. 2022; Rafatullah et al. 2010; Slama et al. 2021). Its extensive use leads to the discharge of MB-containing wastewater, posing a severe threat to both human health and the environment due to its toxic and mutagenic properties (Al-Tohamy et al. 2022). The persistence of MB in aquatic ecosystems can disrupt aquatic life and hinder water treatment processes, making its removal a critical environmental concern (Oladoye et al. 2022). Conventional methods for MB removal, such as adsorption, coagulation, and chemical degradation, encounter challenges, particularly when dealing

Responsible Editor: Sami Rtimi

Po-Jung Huang and Yen-Ping Peng makes equal contributions to this research.

✉ Po-Jung Huang
pjhuang@cc.ncu.edu.tw

Yen-Ping Peng
yppeng@mail.nsysu.edu.tw

[1] Institute of Environmental Engineering, National Sun Yat-Sen University, No. 70 Lien-Hai Rd., Kaohsiung 80424, Taiwan, R.O.C.

[2] Department of Chemical and Materials Engineering, National Central University, Taoyuan 320317, Taiwan

[3] Department of Civil Engineering, National Chi Nan University, Puli, Nantou 54561, Taiwan

with high concentrations of MB (Fito et al. 2023; Rapo and Tonk 2021; Senthilkumaar et al. 2005). Therefore, there is an urgent need to develop new and effective methods for the removal of high concentrations of MB from wastewater.

Photocatalytic degradation using semiconductor materials has emerged as a promising approach for wastewater treatment, offering advantages such as high efficiency, environmental friendliness, and versatility (Huang et al. 2018a; Kumari et al. 2023; Wu et al. 2020). Among various photocatalysts, MOFs and COFs have received significant attention due to their unique properties such as high surface area, tunable pore sizes, and diverse functional groups (Ghosh et al. 2020; Krishnaraj et al. 2020; Younas et al. 2020; Zhang et al. 2022). However, the practical application of MOFs and COFs as photocatalysts has been limited due to their poor photoactivity and stability under visible light irradiation (Gao et al. 2021).

To overcome these limitations, various strategies have been employed, including doping with metallic or non-metallic elements, surface functionalization, and hybridization with other materials (Li et al. 2019; Wang et al. 2020). Recently, research has focused on combining the advantages of MOFs and COFs by developing MOF/COF hybrid materials, which can improve their photocatalytic performance and stability (Li et al. 2019). For instance, a MOF/COF hybrid material composed of UiO-66-NH_2 and BiOBr was found to exhibit high photocatalytic activity for the degradation of RhB under visible light irradiation (Bibi et al. 2018). Another study reported the synthesis of a MOF/COF hybrid material based on NH_2-MIL-125 (Ti) MOF and TTB-TTA COF, which showed excellent photocatalytic activity for the degradation of methyl orange under visible light irradiation (He et al. 2019). Recently, H_2O_2-assisted hybridization of MOFs and COFs has attracted considerable attention as a promising strategy to improve their photocatalytic performance. H_2O_2, as an oxidizing agent, can generate hydroxide radicals and increase the concentration of active sites on the surface of MOFs and COFs, leading to enhanced photocatalytic activity (Islam et al. 2015; Quang et al. 2020; Ren et al. 2021).

In this study, we aim to comprehensively evaluate the photocatalytic capability of a recently synthesized NH_2-MOF-5/MCOF hybrid material, which is subsequently modified to significantly enhance its effectiveness for the degradation of MB under visible light irradiation (Firoozi et al. 2020) and additionally improve its photocatalytic performance by utilizing hydrogen peroxide (H_2O_2) as a co-catalyst. The photocatalytic mechanism, reusability, and stability of the hybrid material and applicability for the other organic pollutants are also investigated in detail. To the best of our knowledge, this is the first report on the use of H_2O_2-assisted MOF/COF hybrid material as a visible-light-driven photocatalyst for methylene blue dye degradation, and this could offer a new approach for the treatment of high concentrations of MB in wastewater. Moreover, our work provides valuable insights into the design and development of MOF/COF hybrid materials with enhanced photocatalytic performance for the degradation of other organic pollutants.

Materials and methods

Materials

All chemicals and reagents were used without additional purification and purchased from commercial suppliers as follows. Zinc acetate dihydrate ($Zn(CH_3CO_2)_2$•$2H_2O$, Merck Millipore), terephthalic acid (H_2BDC, Acros Organics, 98%), melamine ($C_3H_6N_6$, Alfa Aesar, 99%), dimethylformamide (DMF, Acros Organics, 99%), 2-aminoterephthalic acid (NH_2-H_2BDC,Thermo Scientific, 99%), triethylamine ($(C_2H_5)_3N$, Sigma-Aldrich, 99%), ibuprofen, tert-butyl alcohol (TBA, $C_4H_{10}O$, CARLO ERBA Reagent GmbH, 99.5%,), sodium oxalate ($Na_2C_2O_4$ Union Chemical Works Ltd., 99.0%), chloroform($CHCl_3$, Thermo Scientific, 99.9%), acetonitrile (Honeywell, ≥ 99.9%), acetic acid (J.T.Baker, 99.5%), hydrogen peroxide (H_2O_2, Sigma-Aldrich,30% (w/w) in H_2O), dimethyl sulfoxide (DMSO, Sigma-Aldrich, 99%), ethanol (C_2H_5OH, ECHO CHEMICAL CO., LTD, ≥ 99.5%), methanol (CH_3OH, Sigma-Aldrich, ≥ 99.8) Terephthalaldehyde (TA, Alfa Aesar, 98%), and methylene blue ($C_{16}H_{18}N_3ClS$, Sigma Aldrich).

Synthesis of MOF-5

The synthesis of MOF-5 was conducted using a straightforward method (Firoozi et al. 2020). In brief, 0.5 g of terephthalic acid was dissolved in 60 mL of DMF, and 2.19 g of $Zn(CH_3CO_2)_2{\cdot}2H_2O$ was subsequently added to the solution and stirred for 10 min. The resulting mixture was then transferred to Teflon-lined stainless-steel autoclave and heated at 100 °C for 12 h. After the heating process, the solid material that formed was collected, centrifuged, washed with ethanol, and then dried at room temperature. Figure 1a illustrates the synthesis procedure of MOF-5.

Synthesis of NH_2-MOF-5

NH_2-MOF-5 was synthesized according to the literature with slight modifications (Cai et al. 2020). Briefly, 1.288 g of $Zn(NO_3)_2$•$6H_2O$ and 0.288 g of 2-aminoterephthalic acid were added to 40 mL DMF solvent and mixed by ultrasonication in a 100-mL beaker for 5–10 min. Then, the resultant solution was put on a magnetic stirrer, and simultaneously, 2.2 mL of triethylamine was added dropwise, and the mixture was further stirred for 2 h. The residue was collected, centrifuged, and

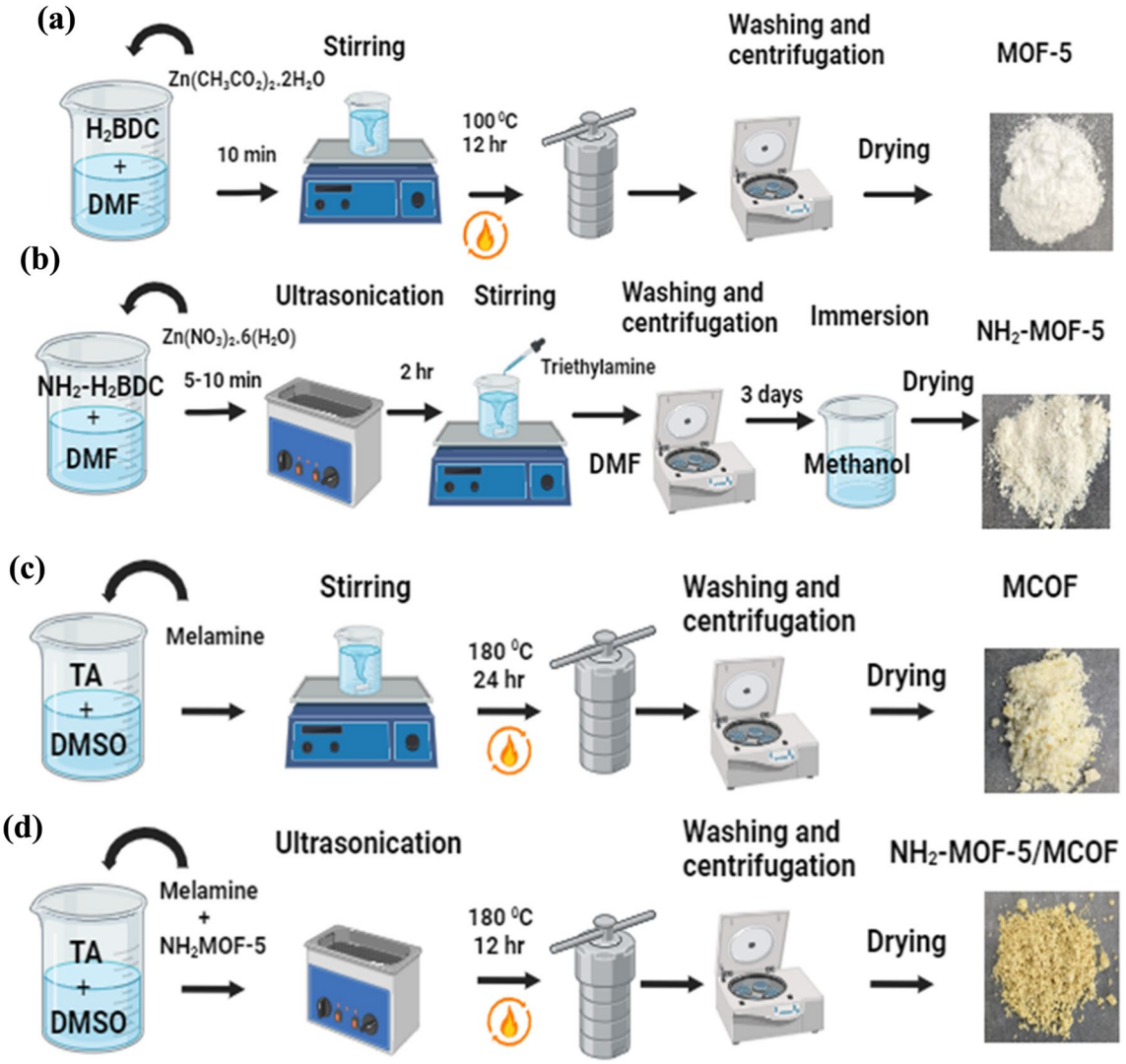

Fig. 1 Schematic diagram of synthesis procedures for **a** MOF-5, **b** NH_2-MOF-5, **c** MCOF, and **d** NH_2-MOF-5/MCOF

washed with DMF. Then, the collected residue was immersed in methanol for 3 days and the methanol solution was changed every 24 h. Ultimately, the obtained white product was dried at 120 °C and used for further analysis. Figure 1b illustrates the synthesis procedure for MOF-5-NH_2.

Synthesis of melamine-rich COF (MCOF)

Melamine-rich COF was synthesized using the hydrothermal method. Briefly, 0.25 g of melamine and 0.5 g of terephthaldehyde were added to 25 mL DMSO. The solution was placed on a magnetic stirrer and mixed until a homogeneous solution. The obtained solution was transferred into a Teflon-lined stainless-steel autoclave and calcinated to 180 °C for 24 h. Finally, the resultant precipitate was centrifuged, washed with DI water, and dried at 80 °C for 12 h. Figure 1c depicts the synthesis process for MCOF.

Preparation of NH_2-MOF-5/MCOF

NH_2-MOF-5/MCOF hybrid was synthesized according to the literature with slight modifications (Firoozi et al. 2020). 0.2 g of NH_2-MOF-5, 0.5 g of melamine, 0.5 g of terephthaldehyde, and 5 mL of water were added to 25 mL DMSO. The solution was mixed using ultrasonication. Later, it was transferred to a Teflon-lined stainless-steel autoclave and calcinated at 180 °C for 12 h. Finally, the formed precipitate was collected, centrifuged, washed with ethanol, and dried at 60 °C. Figure 1d shows the synthesis method for NH_2-MOF-5/ MCOF. Additionally, Fig. S1 illustrates the proposed structure of NH_2-MOF-5/MCOF.

Characterization

The structural characteristics of the MOF/COF hybrid were analyzed using Fourier transform infrared (FT-IR) spectroscopy (Nicolet iS5 FT-IR spectrometric analyzer using KBr powder). The morphological characteristics were studied using X-ray diffraction (XRD, Bruker D8) and scanning electron microscopy (SEM, JEOL-6330). The chemical composition and electronic states of the material's surface were identified using X-ray photoelectron spectroscopy (XPS, VG Scientific ESCALAB 250). Surface area and porosity analyzer (Micromeritics ASAP 2460) was used to determine the surface area and pore characterization of MOF/COF hybrid. To analyze the band gap of the MOF/COF material, UV–vis diffuse reflectance spectroscopy (DRS) was performed using a UV-DRS (V-750) spectrophotometer with $BaSO_4$ as a reference. These techniques provided a comprehensive understanding of the structural, morphological, and electronic properties of the MOF/COF hybrid material.

Photocatalytic experiment

Photocatalytic experiments were performed to investigate the efficacy of MOF/COF hybrid as a potential photocatalyst for the degradation of methylene blue (MB) dye. The experiments were carried out separately under visible light (5 W LED, 400–700 nm) and UV light (100-W mercury (Hg) vapor lamp, 365 nm) at room temperature. The light source was positioned 10 cm away from the reaction mixture to ensure uniform illumination.

Before initiating the photocatalytic reaction, the mixture solution was magnetically stirred for 1 h in the dark to ensure that adsorption–desorption equilibrium was reached between the dye and the material. This ensured that any dye adsorbed onto the surface of the MOF/COF hybrid was desorbed and released into the solution prior to initiating the reaction.

For the photodegradation of MB dye, different dosages of the MOF/COF hybrid were added to various concentrations of 25 mL MB solutions ranging from 5 to 100 mg L^{-1}. The mixtures were kept under UV or visible light throughout the reaction time. A 3-mL sample was taken at specific time intervals, and the concentration of the dye was analyzed using a UV–visible spectrophotometer (HITACHI U-2900) for recording the maximum absorbance wavelength of MB (λ_{max}) at 664 nm.

In order to accelerate the photocatalytic degradation of MB, various concentrations of H_2O_2 were added to the mixture as an accelerator. The photoremoval of MB was calculated using the following equation:

$$\text{Photodegradation efficiency } (\%) = \frac{C_0 - C}{C_0} \times 100 \quad (1)$$

where C_0 (mg L^{-1}) denotes the initial concentration and C (mg L^{-1}) represents the final MB concentration.

The experimental setup was designed to ensure that the photocatalytic experiments were conducted under controlled conditions and that the results obtained were reliable and reproducible.

Results and discussion

SEM analysis

Figure 2a shows the SEM image of synthesized MOF-5, which consists of irregular flaky particles that tend to aggregate due to the absorption of water molecules, with sizes ranging from 2 to 4 µm (Chen et al. 2019). The SEM image in Fig. 2b confirms NH_2-MOF-5's spherical particle morphology at the nanoscale (240 nm) with a smooth surface, aligning with previous studies (Yan et al. 2022). Figure 2c shows the SEM images of MCOF, illustrating the porous structure with interlinking randomness particles (Periyasamy and Viswanathan 2019). Moreover, the SEM images of NH_2-MOF-5/MCOF are shown in Fig. 2d, indicating that smooth spherical-shaped material of NH_2-MOF-5 has altered to a rough surface with well-dispersed MCOF materials with average particle size 300 nm (Firoozi et al. 2020). It is noteworthy that, despite maintaining the same particle morphology as NH_2-MOF-5, the hybrid material exhibits a slight increase in average size due to the integration of MCOF. This observation is consistent with previous studies on the synthesis of aza-MOF@COF (Peng et al. 2020).

XRD analysis

Figure 3 shows the X-ray diffraction (XRD) spectra of MOF-5, NH_2-MOF-5, MCOF, and NH_2-MOF-5/MCOF. We obtained microcrystalline MOF-5 particles in good agreement with the experimental data published by Hafizovic et al. (2007), as shown in Fig. 3a (Hafizovic et al. 2007). In Fig. 3b, the NH_2-MOF-5 XRD pattern reveals four characteristic peaks observed at $2\theta = 6.31°$, 9.84°, 13.96°, and 15.44° corresponding to the (0 0 2), (0 2 2), (0 0 4), and (0 2 4) facets, respectively, which were consistent with both the simulated and synthesized MOF-5 (Wang et al. 2018; Wen et al. 2019). The XRD pattern of MCOF, as depicted in Fig. 3c, exhibits a broad peak in the 2θ range from 15 to 30°, centered at 21.34°, indicating an amorphous structure with a low degree of crystallinity, consistent with findings in the literature (Foulady-Dehaghi and Sohrabnezhad 2021).

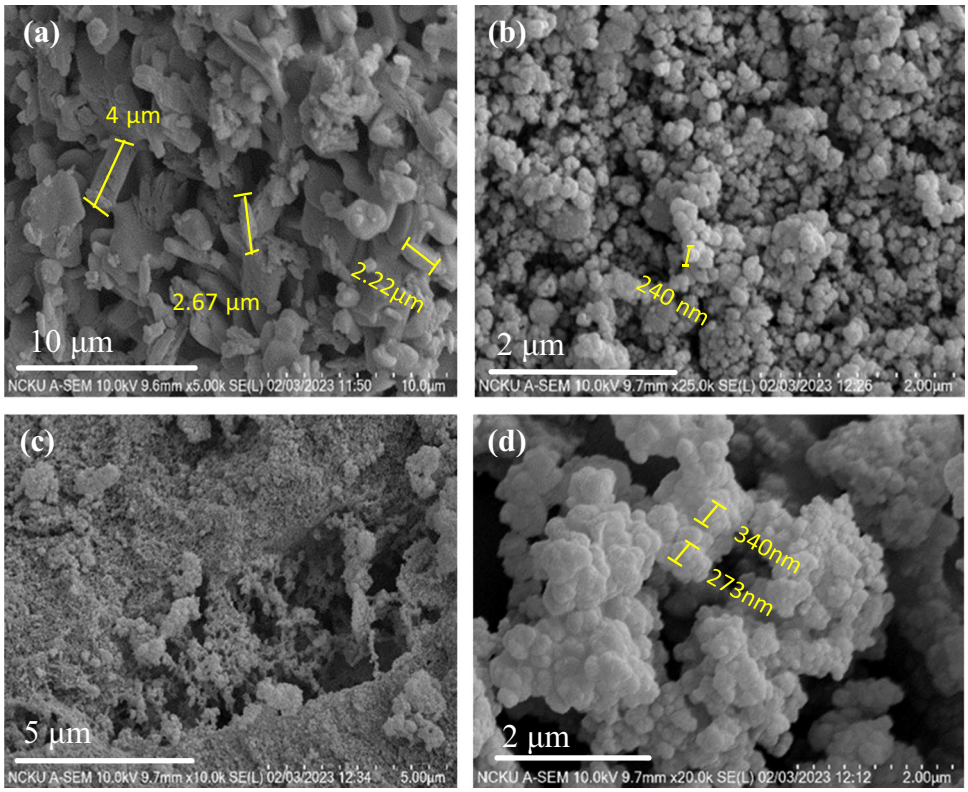

Fig. 2 SEM images of **a** MOF-5, **b** NH_2-MOF-5, **c** MCOF, and **d** NH_2-MOF-5/MCOF

The XRD pattern of the synthesized NH_2-MOF-5/MCOF hybrid material, as shown in Fig. 3d, displays a broad peak similar to MCOF due to the weak intensity of NH_2-MOF-5, indicating the successful retention of the parent MCOF structure (He et al. 2019). Additionally, low-intensity peaks from MOFs are also clearly observed, overlapping with MCOF signals, indicating the successful synthesis of the NH_2-MOF-5/MCOF hybrid material based on the analyses presented above (Holder and Schaak 2019).

FT-IR analysis

Figure 4 displays the FT-IR spectra of terephthalic acid, MOF-5, NH_2-MOF-5, MCOF, and the NH_2-MOF-5/MCOF hybrid material. FT-IR spectrum of the terephthalic acid (Fig. 4a) shows strong asymmetric vibration of COO group at 1697 cm^{-1} (Tellez et al. 2001). Due to formation of the large MOF-5 structure and the interaction between Zn atom with COO bond results, this carboxyl band shifted to lower frequency values (Kayan and Kayan 2021). In the MOF-5 FT-IR spectrum (Fig. 4b), these characteristic carboxyl group absorption peaks at approximately 1378 and 1605 cm^{-1} are assigned to the symmetric O = C-O and asymmetric O = C-O bonded to Zn, respectively (Hadjiivanov et al. 2021). While the absorption peak at 537 cm^{-1} is attributed to the Zn–O stretching vibration (Cai et al. 2020). The absorption peak at 3430 cm^{-1} in the MOF-5 structure corresponds to the O–H stretching vibration originating from H_2O molecules adsorbed by the MOF. Similar to MOF-5, NH_2-MOF-5 exhibits asymmetric and symmetric carboxyl absorption peaks appearing at 1579 and 1369 cm^{-1} (Fig. 4c). In contrast to MOF-5, NH_2-MOF-5 exhibits new, less intense absorption peaks at 3418 and 3370 cm^{-1}, which are ascribed to N–H stretching vibrations (Wen et al. 2019). The MCOF FT-IR spectrum (Fig. 4d) displays two absorption bands at 1543 and 1352 cm^{-1}, corresponding to the aromatic C-N stretching vibration originating from the heterocyclic triazine ring of melamine (Periyasamy and Viswanathan 2019). The broad absorption peak at approximately 3465 cm^{-1} is attributed to the O–H stretching vibration derived from H_2O molecules adsorbed by the MCOF. Two additional absorption peaks at 1017 and 813 cm^{-1} are assigned to the aromatic C-H and cyclic C-N asymmetric vibration, respectively (Periyasamy and Viswanathan 2019). The resulting NH_2-MOF-5/MCOF hybrid FT-IR spectrum (Fig. 4e) exhibits new and unique absorption peaks at approximately 1552, 1483, and 1345 cm^{-1}, corresponding to C = N, C = C, and C-N stretching vibrations, respectively. These observations confirm the successful synthesis of the hybrid material.

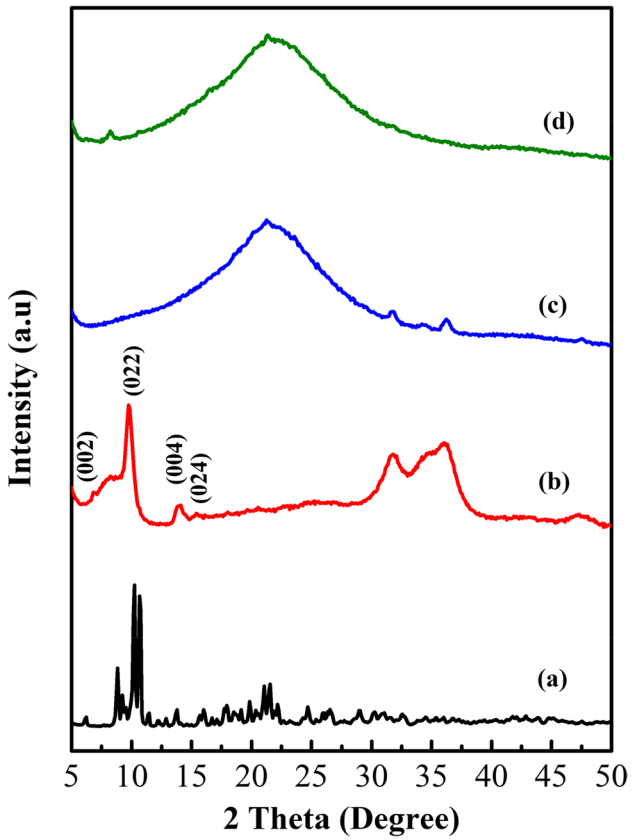

Fig. 3 XRD images of **a** MOF-5, **b** NH_2-MOF-5, **c** MCOF, and **d** NH_2-MOF-5/MCOF

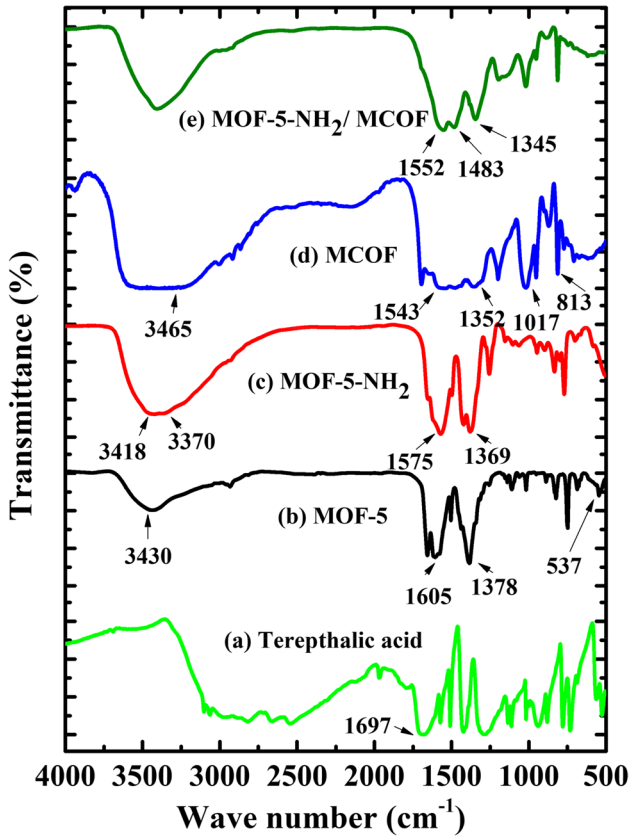

Fig. 4 FT-IR spectra of **a** Terephthalic acid, **b** MOF-5, **c** NH_2-MOF-5, **d** MCOF, and **e** NH_2-MOF-5/MCOF

XPS analysis

Figure 5 presents the results of X-ray photoelectron spectroscopy (XPS) measurements for the synthesized NH_2-MOF-5/MCOF hybrid material. As shown in Fig. 5a, the XPS spectra confirmed the presence of C, N, O, and Zn elements in the hybrid material. Furthermore, the C 1 s deconvoluted XPS spectra (Fig. 5b) exhibited three well-distinguished peaks, which were assigned to the C = C bond, C = N bond, and C-N bond, respectively, with their respective binding energies of 284.9 eV, 287.1 eV, and 287.7 eV (Yan et al. 2004). Similarly, the N 1 s deconvoluted XPS spectra (Fig. 5c) displayed two separate peaks at 398.2 eV and 399.4 eV, which were attributed to the C-N bond and C = N bond, respectively (Yan et al. 2004). The peak at 531.7 eV in the O 1 s XPS spectra (Fig. 5d) confirmed the formation of the Zn–O bond (Gadipelli and Guo 2014). Additionally, two peaks at 1022.3 eV and 1045.3 eV were observed in the Zn 2p XPS spectra (Fig. 5e) and were ascribed to the 2p 3/2 and 2p 1/2 states of Zn 2p (Peng et al. 2014). The observed XPS results were consistent with the FT-IR results and confirmed the successful formation of the NH_2-MOF-5/MCOF hybrid material.

UV–vis diffuse reflectance spectra and Tauc plot analysis

Figure 6a and b shows the UV–vis spectrum and Tauc plot of the as-synthesized materials. The band gap energy (E_g) for each material was determined using the Tauc method outlined below (Makuła et al. 2018).

$$(\alpha.h\nu)^{1/\gamma} = B\left(h\nu - E_g\right) \quad (2)$$

where α represents the absorption coefficient, $h\nu$ stands for photon energy, and E_g represents the band gap energy, while B denotes a constant. The γ factor, determined by the nature of electron transitions, is set to 1/2 for direct transition band gaps and 2 for indirect transition band gaps. MOF-5 demonstrated an absorption peak at around 290 nm and an absorption edge at 364 nm, which falls under the UV region, corresponding to the band gap of 3.57 eV (Fiaz et al. 2021; Muller et al. 2011; Yang et al. 2014). This observation confirmed the presence of the organic linker terephthalic acid and the inorganic Zn metal cluster, both of which contribute to ligand-to-metal charge transfer (LMCT) (Fiaz et al. 2021). Moreover, the UV–vis spectrum investigation

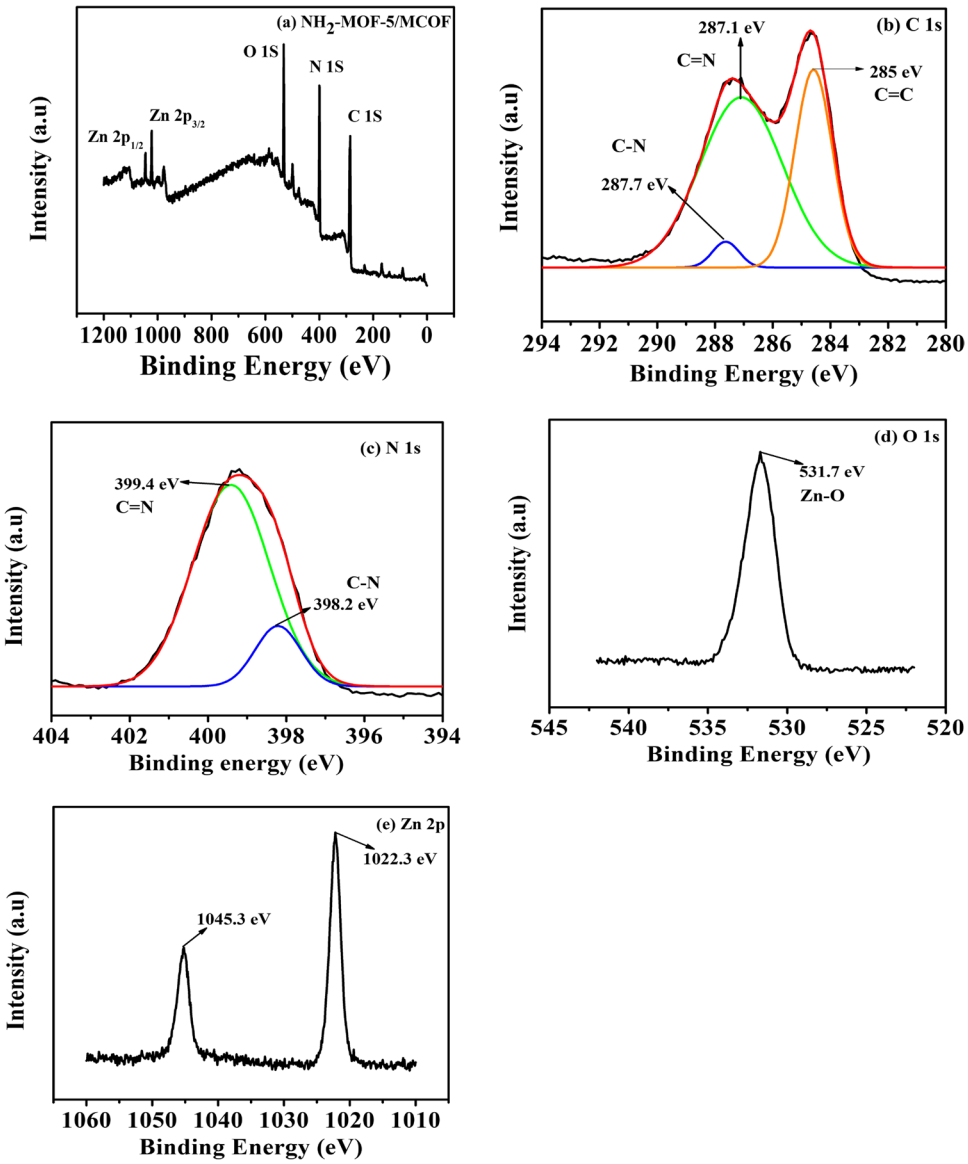

Fig. 5 XPS results of NH_2-MOF-5/MCOF: **a** survey spectrum; **b** C 1 s; **c** N 1 s; **d** O 1 s; and **e** Zn 2p

of the synthesized MCOF material revealed an absorption edge at 432 nm which falls under visible region, corresponding to a band gap of 3.20 eV. This observation indicates a high degree of delocalization and conjugation within the melamine and phenyl polymeric structure (Huang et al. 2018b). The addition of amine functionality to MOF-5 (i.e., NH_2-MOF-5) caused the absorption edge to red shift to 445 nm, which falls within the visible region. The Tauc plot analysis further demonstrated a much lower band gap of 2.76 eV (Fiaz et al. 2021). Consequently, the resulting NH_2-MOF-5/MCOF material exhibited a significant red shift in the absorption edge to 596 nm, with a very low band gap of 2.20 eV. This is mainly due to the enhanced conjugation throughout the hybrid structure, allowing for more efficient delocalization of electrons, which in turn reduces the energy gap between the valence and conduction bands, resulting in a lower band gap.

Photocatalytic removal of MB

MB dye was employed as a model contaminant to investigate the photocatalytic activity of the NH_2-MOF-5/MCOF hybrid material. The solution was kept in the dark with constant magnetic stirring for 1 h prior to each photocatalytic experiment to ensure adsorption–desorption equilibrium. After achieving adsorption–desorption equilibrium between NH_2-MOF-5/MCOF hybrid material and MB dye, we evaluate the photocatalytic activity by quantifying the photodegradation of MB dye, using the equilibrium concentration of MB as the initial concentration for our analysis. Previous

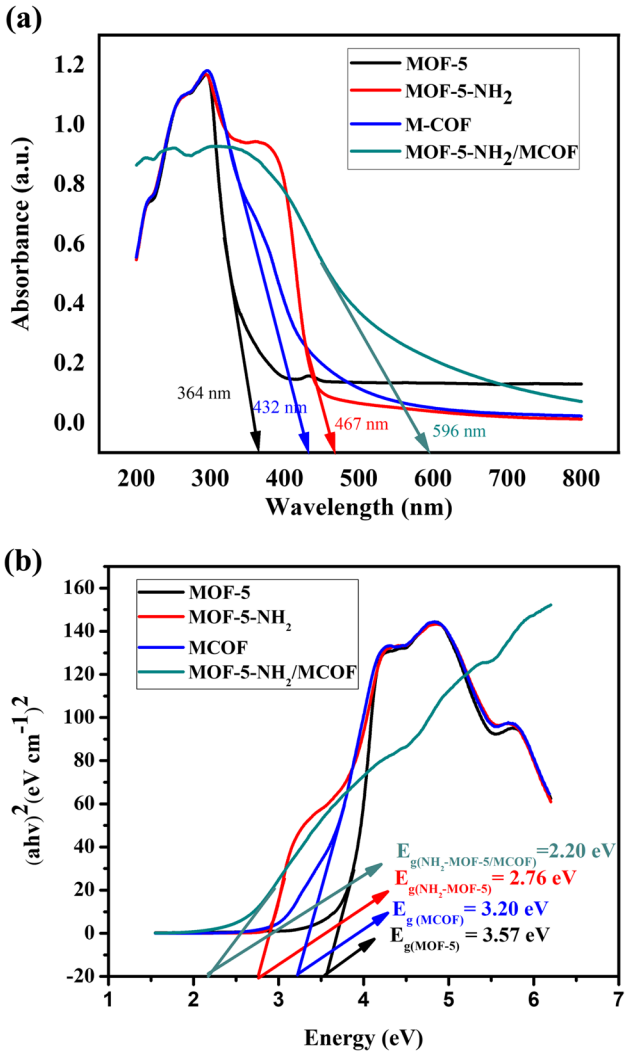

Fig. 6 **a** UV-DRS data of MOF-5, NH_2-MOF-5, M-COF, and NH_2-MOF-5/MCOF and **b** Tauc plot of MOF-5, NH_2-MOF-5, MCOF, and NH_2-MOF-5/MCOF

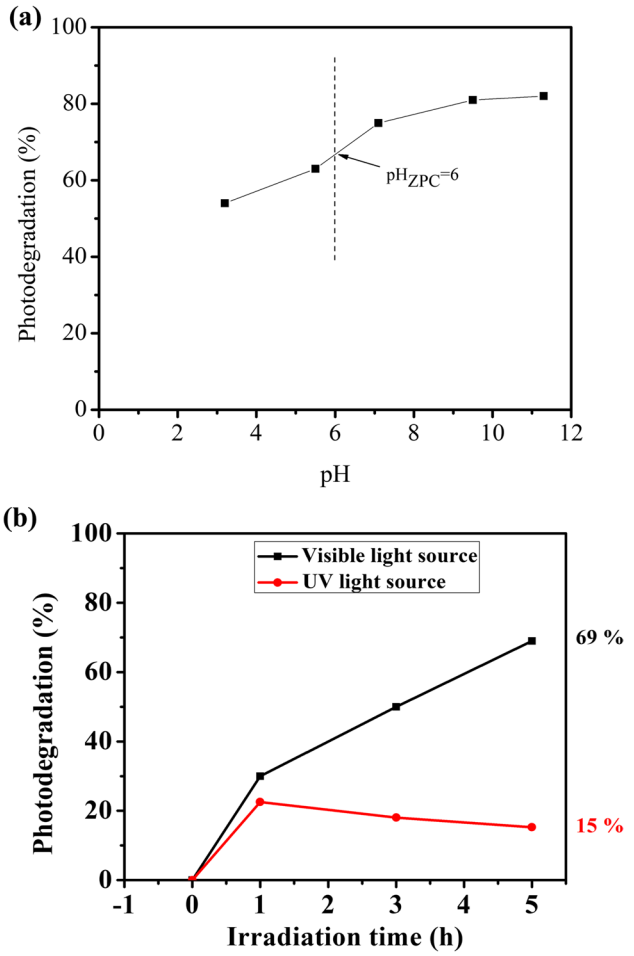

Fig. 7 **a** Photodegradation efficiencies of NH_2-MOF-5/MCOF (20 mg) using 5 mg L^{-1} MB dye under visible light (5 W LED, 400–700 nm) with different pH values (MB volume = 100 mL, irradiation time = 21 h). **b** Photodegradation efficiencies of NH_2-MOF-5/MCOF (60 mg) using 30 mg L^{-1} MB dye under UV light (100 W Hg, 365 nm) and visible light (5 W LED, 400–700 nm) at pH 9.5 (MB volume = 25 mL)

studies have demonstrated that various factors, such as pH and light source parameters, may affect the photocatalytic efficiency of the material (Reza et al. 2015). Figure 7a indicates that the photocatalytic efficiency of the catalyst is significantly better under basic conditions (pH > 7) compared to acidic conditions (pH < 7). This phenomenon can be attributed to the zeta potential value (pH_{zpc}) of the NH_2-MOF-5/MCOF material, which is negative above pH 6 and positive below pH 6 (Firoozi et al. 2020). At pH > 6, positively charged MB is more likely to interact with the negatively charged catalyst, resulting in higher photodegradation of MB dye. Conversely, at pH < 6, repulsion between the positively charged catalyst and positively charged MB leads to a lower photodegradation efficiency of MB. Thus, it can be deduced that under basic conditions, the NH_2-MOF-5/MCOF material exhibits higher photocatalytic ability. We also observed that at pH 9.5, the degradation of MB reaches its highest percentage, and further increases in pH result in degradation percentages that remain relatively constant. Therefore, for subsequent experiments, we have chosen pH 9.5 as our optimum pH condition, as it demonstrates the most efficient degradation of MB. However, the results suggest that a longer irradiation time is required for effective dye degradation. To utilize this material for environmental remediation, we must test it under higher MB dye concentrations and ensure it achieves high degradation efficiency within a short period of time. Therefore, the MB concentration was adjusted to 30 mg L^{-1}, and the catalyst dosage was increased from 0.2 to 2.4 g L^{-1}. Figure 7b shows that irradiation with visible light under basic conditions (pH = 9.5) yielded satisfactory results. Within 5 h of irradiation, the visible light achieved 69% photodegradation of MB dye, whereas the UV light

irradiation resulted in only 15% photodegradation. This observation aligns with the UV DRS data, revealing that the NH_2-MOF-5/MCOF material has two weak absorption bands below 300 nm in the UV region and strong absorption which falls within the visible light spectrum explains low photodegradation under UV light (Gupta et al. 2021). Furthermore, the material's narrow band gap results in limited activity when exposed to UV light, consequently leading to a reduced generation of electron–hole pairs (Keerthana et al. 2021). Therefore, the parameters were optimized for high-concentration MB dye (30 mg L^{-1}) as follows: basic conditions (pH = 9.5), visible light irradiation (420–700 nm), and a catalyst dosage of 60 mg for efficient dye degradation.

A comprehensive comparative analysis of multiple key parameters, including catalyst type, band gap, light source, dye concentration, irradiation time, and degradation efficiency, is meticulously presented in Table 1. Notably, our findings have demonstrated satisfactory outcomes, despite the use of elevated concentrations of MB dye, in line with the existing literature.

Effect of hydrogen peroxide (H_2O_2)–assisted photodegradation

Hydrogen peroxide (H_2O_2) is one of the commonly used oxidants in wastewater treatment. This study investigates the efficiency of photodegradation of MB dye by using H_2O_2-assisted NH_2-MOF-5/MCOF material. Initially, a blank experiment was performed for 5 h under visible light irradiation, which resulted in a 25% photodegradation of MB, as shown in Fig. 8a. The result is ascribed to the ability of MB to absorb visible light in the region of 500–700 nm and undergo self-degradation (Khan et al. 2022; Liu et al. 2012). Figure 8a also shows the results of control experiment that when H_2O_2 was added to the MB solution, hydroxyl radicals were generated in the medium, resulting in a 46% photodegradation. In contrast, by applying NH_2-MOF-5/MCOF as catalysts, 69% of MB removal was achieved in 5 h. Notably, the addition of H_2O_2-assisted NH_2-MOF-5/MCOF material resulted in an 80% photoremoval efficiency within 5 h. The effects of H_2O_2 concentration and initial MB concentration on the photodegradation efficiency of MB were further discussed. Figure 8b shows the photodegradation efficiency of MB increased with the increasing H_2O_2 concentration, with an optimum concentration of 0.06 mol L^{-1} H_2O_2, where the photodegradation efficiency reached 92% within 7 h. Figure 8c illustrates the photodegradation of different MB concentrations by adding NH_2-MOF-5/MCOF-assisted 0.06 mol L^{-1} H_2O_2. Results showed that 11.75 mg L^{-1} MB was photodegraded by 90% within 3 h, while 30 mg L^{-1} MB and 83 mg L^{-1} MB were photodegraded by 92% and 57% within 7 h, respectively. These results demonstrate the effectiveness of H_2O_2-assisted NH_2-MOF-5/MCOF material in treating high concentrations of MB dye photodegradation.

It is also worth noting that the initial MB concentrations showed a reduction after 1 h of dark treatment, indicating the hybrid material's effective adsorption capability, as depicted in Fig. S2. However, after 1 h, it has reached to adsorption–desorption equilibrium. Specifically, during dark treatment for 1 h, the initial concentrations of 25 mg L^{-1} MB decreased to 11.75 mg L^{-1}, 50 mg L^{-1} MB decreased to 30 mg L^{-1}, and 100 mg L^{-1} MB decreased to 83 mg L^{-1}, illustrating the material's adsorption ability to remove MB from the solution (Figs. S2, S3). This observed synergy emphasizes the heightened effectiveness of the H_2O_2-assisted NH_2-MOF-5/MCOF material when both adsorption and photocatalytic processes collaborate. However, it is crucial to acknowledge that the material's moderately low Brunauer–Emmett–Teller (BET) surface area, as illustrated in Fig. S4 and Table S1, limits the efficacy of adsorption alone, particularly for higher concentrations such as 25 mg L^{-1} MB or above. In such cases, the dominant and more effective process shifts towards photocatalytic activity.

Table 1 Comparison of the removal of methylene blue dye by different materials

Material	Dye	E_g (eV)	Light source	Dye conc. (mg L^{-1})	Time (min)	Degradation efficiency (%)	Ref
Cd MOF-CdS	MB	3.15	UV	20	100	91.9	(Jing et al. 2022)
Ni/Co-MOF	MB	2.88	Vis	20	120	71.20	(Shan et al. 2022)
Ni-MOF/BiOBr	MB	3.08	Vis	20	120	82.80	(Ma et al. 2023)
$(emim)_2[InK(btec)_{1.5}(H_2O)_2]$	MB	3.15	UV	5	180	90	(Ji et al. 2012)
Cu_3 (4-bpah)$_4$ (1,3,5-btc)$_2$]•$8H_2O$	MB	-	UV	10	240	50	(Zhou et al. 2012)
Zn_2(tkcomm)(llpd)$_2$	MB	3.26	UV	16	90	78	(Guo et al. 2012)
NH_2-MIL-88B(Fe) (50) + H_2O_2	MB	1.14	Vis	30	120	57	(Li et al. 2017)
NH_2-MOF-5/MCOF + 0.06 mol L^{-1} H_2O_2 (100 µL)	MB	2.20	Vis	11.75	180	90	This work
NH_2-MOF-5/MCOF + 0.06 mol L^{-1} H_2O_2 (100 µL)	MB	2.20	Vis	30	420	92	This work
NH_2-MOF-5/MCOF + 0.06 mol L^{-1} H_2O_2 (100 µL)	MB	2.20	Vis	83	420	57	This work

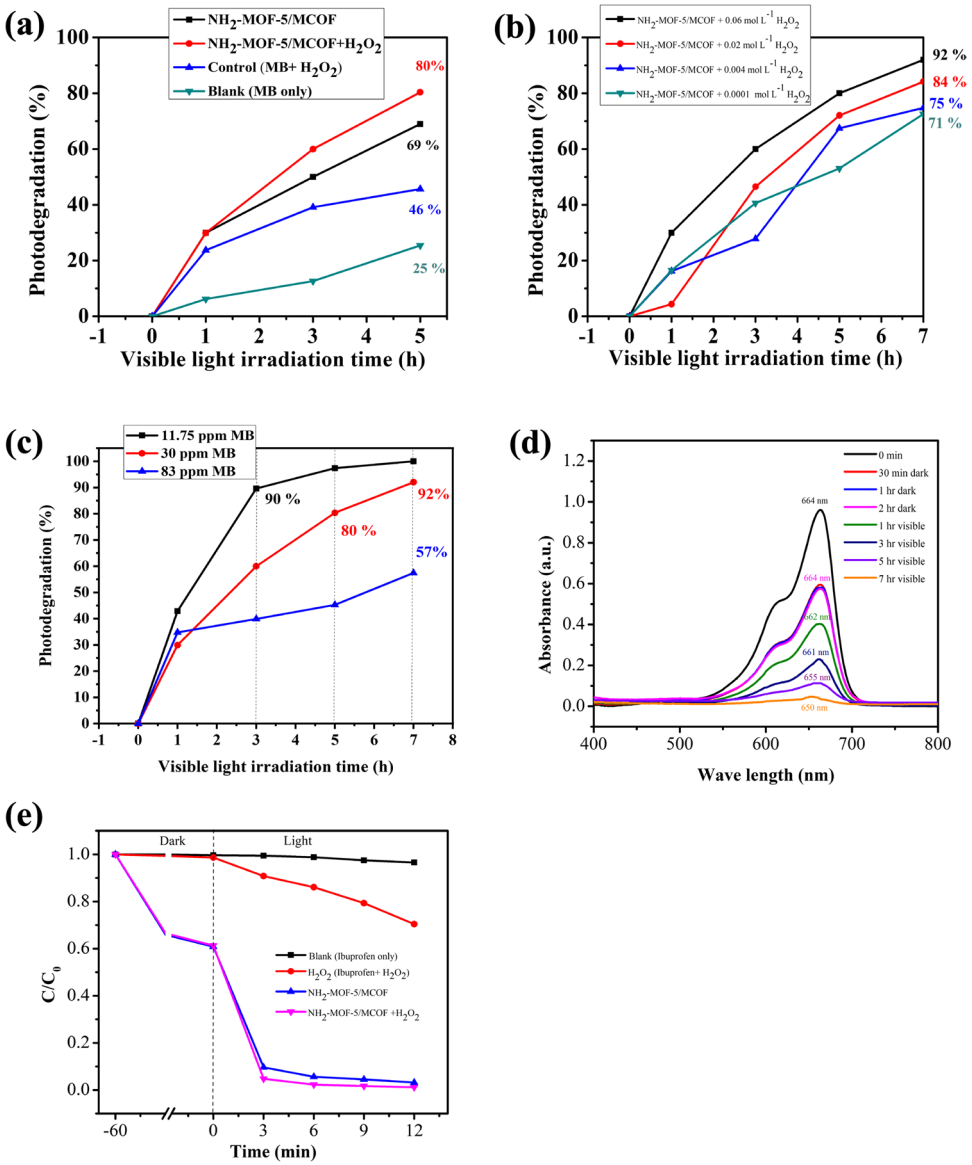

Fig. 8 **a** Photodegradation of 30 mg L^{-1} MB dye (25 mL) in the presence of NH_2-MOF-5/MCOF, NH_2-MOF-5/MCOF-assisted 0.06 mol L^{-1} H_2O_2, control (MB + 0.06 mol L^{-1} H_2O_2), and blank (MB only) at pH 9.5 (light source—5 W LED, 400–700 nm). **b** Photodegradation of 30 mg L^{-1} MB dye (25 mL) in the presence of NH_2-MOF-5/MCOF + 0.06 mol L^{-1} H_2O_2, NH_2-MOF-5/MCOF + 0.02 mol L^{-1} H_2O_2, NH_2-MOF-5/MCOF + 0.004 mol L^{-1} H_2O_2, and NH_2-MOF-5/MCOF + 0.0001 mol L^{-1} H_2O_2 at pH 9.5 (light source—5 W LED, 400–700 nm). **c** Photodegradation of 11.75 mg L^{-1} MB, 30 mg L^{-1} MB, and 83 mg L^{-1} MB dye in the presence NH_2-MOF-5/MCOF-assisted 0.06 mol L^{-1} H_2O_2 at pH 9.5 (MB volume = 25 mL, light source—5 W LED, 400–700 nm). **d** UV–visible absorption spectra of 30 mg L^{-1} MB dye in the presence of NH_2-MOF-5/MCOF-assisted 0.06 mol L^{-1} H_2O_2 at pH 9.5 (MB volume = 25 mL, light source—5 W LED, 400–700 nm). **e** Photodegradation of 3.3 mg L^{-1} ibuprofen dye (25 mL) in the presence of blank (Ibuprofen only), H_2O_2 (MB + 0.06 mol L^{-1} H_2O_2), NH_2-MOF-5/MCOF, and NH_2-MOF-5/MCOF-assisted 0.06 mol L^{-1} H_2O_2, at pH 4 (light source—5 W LED, 400–700 nm)

We also observed some interesting phenomena in the MB photocatalytic degradation process. Figure 8d illustrates that as the visible light irradiation time increases, the maximum absorbance wavelength of MB shifts from 664 to 650 nm. This shift towards lower values, known as a hypsochromic shift, indicates the formation of reaction intermediates (Marban et al. 2011; Matalkeh et al. 2022).

We further explored the broad applicability of our H_2O_2-assisted NH_2-MOF-5/MCOF hybrid by employing ibuprofen, a widely consumed pharmaceutical and personal care product, as our model pollutant to assess photocatalytic activity under visible light. The experimental procedure and analytical method used to detect ibuprofen are described in Text S1. Results revealed that in the absence of catalyst, only

3% of ibuprofen was removed, while H_2O_2 alone removed 30% within 12 min. However, upon introducing NH_2-MOF-5/MCOF, a remarkable 97% removal of ibuprofen was achieved, indicating the excellent photocatalytic nature of the hybrid material. Furthermore, when H_2O_2-assisted NH_2-MOF-5/MCOF was used, 99% of ibuprofen was removed within the same time frame, demonstrating the enhanced photocatalytic activity of the material in the presence of H_2O_2. It is worth noting that both adsorption and photodegradation contribute to the removal of ibuprofen. Specifically, adsorption accounts for 39% of the removal, while photocatalytic degradation constitutes the majority, contributing 60% (Fig. S5).

Kinetic study

Table 2 presents the results of the kinetic analysis conducted for the photodegradation of MB. These analyses were performed to determine the reaction rate order. The obtained R^2 values suggest that the degradation of MB can be effectively described by pseudo-first-order kinetics, as evidenced by the high linearity of the relationship with an R^2 value of 0.983 (Alkaykh et al. 2020; Jawad et al. 2018). The pseudo-first-order rate equation used for this analysis is expressed as follows, where C_0 represents the initial concentration, C denotes the final concentration, t is the reaction time (h), and k stands for the pseudo-first-order rate constant (h^{-1}).

$$\ln\frac{C_0}{C} = kt \tag{3}$$

Table 2 Optimizing rate order for MB dye degradation with NH_2-MOF-5/MCOF catalyst

Weight of the catalyst (NH_2MOF-5/MCOF) (mg)	H_2O_2 concentration (mol L^{-1})	Concentration of the MB dye (mg L^{-1})	Volume of the solution (mL)	Rate order	R^2 value
60	0.06	30	25	0	0.954
60	0.06	30	25	1	0.983
60	0.06	30	25	2	0.562

Further analysis was conducted to evaluate the effects of different MB concentrations and the addition of H_2O_2 on the rate of MB degradation using NH_2-MOF-5/MCOF material (60 mg). Table 3 summarizes comparison of the pseudo-first-order rate constants and R^2 value with 60 mg NH_2-MOF-5/MCOF material and different MB and H_2O_2 concentrations. The highest rate (0.728 h^{-1}) was observed for 11.75 mg L^{-1} MB using both catalyst and H_2O_2 together. For 30 mg L^{-1} MB degradation, the rate was 0.099 h^{-1} using only catalyst, whereas adding H_2O_2 (0.06 mol L^{-1}) significantly increased the rate to 0.342 h^{-1}, almost 3.5 times higher. This highlights the crucial role of H_2O_2 as an accelerator for MB degradation using NH_2-MOF-5/MCOF. In addition, when using 83 mg L^{-1} MB, the degradation rate decreased to 0.118 h^{-1}. It is evident that increasing the concentration of MB resulted in a corresponding decrease in the degradation rate.

Photocatalytic mechanism

To gain a comprehensive understanding of the photocatalytic mechanism of the NH_2-MOF-5/MCOF material, it is crucial to determine the conduction band (CB) and valence band (VB) positions of both NH_2-MOF-5 and MCOF individually. Previous studies have demonstrated that analyzing Mott–Schottky (M-S) plots for both NH_2-MOF-5 and MCOF materials reveals a positive slope, indicating they belong to n-type semiconductors (Rajan et al. 2024; Wan et al. 2022). In their study, Rajan et al. demonstrated that utilizing the Mott–Schottky (M-S) plot for NH_2-MOF-5 material yielded a calculated flat band potential of − 0.49 eV vs. NHE (Rajan et al. 2024). For n-type semiconductors, the conduction band (CB) potential is typically 0.1 eV lower than the flat band potential; thus, the CB potential for NH_2-MOF-5 is calculated to be − 0.59 eV vs. NHE (Kalanur 2019). By applying the band gap equation $E_g = E_{VB} - E_{CB}$ and considering the UV-DRS data which revealed an E_g value of 2.76 eV for NH_2-MOF-5, the valence band (VB) potential is calculated to be 2.17 eV vs. NHE. Liu et al. calculated the VB potential as 1.45 eV vs. NHE through analysis of the VB-XPS spectra of the MCOF material (Liu et al. 2023). According the above band gap equation, we can calculate the CB potential of MCOF = − 1.75 e vs. NHE.

Table 3 Comparison of the first-order rate constant and R^2 value with NH_2-MOF-5/MCOF material and different MB and H_2O_2 concentrations

Weight of the Catalyst (NH_2-MOF-5/MCOF) (mg)	Concentration of the MB dye (mg L^{-1})	H_2O_2 concentration (mol L^{-1})	Volume of the solution (mL)	1st-order rate constant (k_1) (h^{-1})	R^2 value
60	11.75	0.06	25	0.728	0.995
60	30	0.06	25	0.342	0.983
60	30	0	25	0.099	0.982
60	83	0.06	25	0.118	0.940

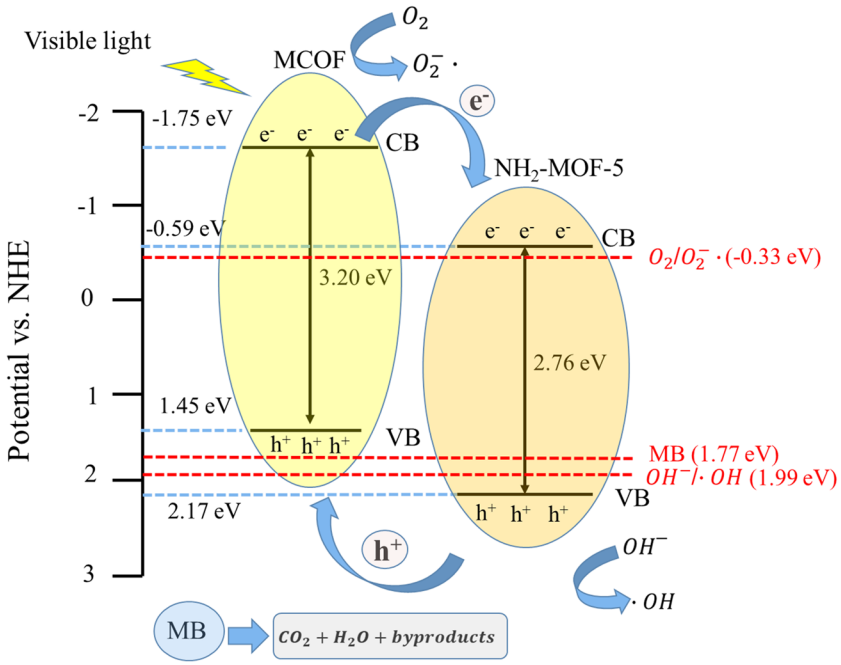

Fig. 9 Energy band diagram of NH_2-MOF-5/MCOF

Based on the calculated band values for each NH_2-MOF-5 and MCOF individually, we have illustrated the energy band diagram as shown in Fig. 9. The mechanism for heterojunction NH_2-MOF-5/MCOF photocatalytic degradation was proposed (Qian et al. 2019; Saha et al. 2018). Under visible light radiation, both NH_2-MOF-5 and MCOF are excited due to their narrow band gap, resulting in the formation of electron (e^-) and hole (h^+) pairs (Eq. 4). Since the conduction band (CB) potential of MCOF (− 1.75 eV vs. NHE) is more negative than that of NH_2-MOF-5 (− 0.59 eV vs. NHE), electrons generated in the CB of MCOF transfer to the CB of NH_2-MOF-5. Similarly, holes produced from the more positive VB of NH_2-MOF-5 (2.17 eV vs. NHE) transfer to the less positive VB of MCOF (1.45 eV vs. NHE). These holes act as strong oxidizing agents and can directly react with the MB dye molecule since the redox potential of MB (1.77 eV vs. NHE) is lower than that of NH_2-MOF-5 (2.17 eV vs. NHE), degrading into CO_2, H_2O, and other byproducts (Eq. 9). Additionally, the holes can react with hydroxide ions (OH^-) to initiate hydroxyl radicals (•OH), which further participate in the dye degradation reaction (Eq. 5). Furthermore, since the CB potential of MCOF is more negative (− 1.75 eV vs. NHE) than the standard redox potential of $O_2/O_2^-\cdot$ (− 0.33 eV vs. NHE), the photoexcited electron in the conduction band (e^-) reacts with dissolved oxygen (O_2) to generate super oxide radicals (O_2^-•) (Eq. 6), which also contribute to the dye degradation reaction (Eq. 9). The photocatalytic degradation of MB by NH_2-MOF-5/MCOF is increased by 3.5-fold in the presence of H_2O_2. The role of H_2O_2 can be explained using the advanced oxidation process (AOP), where the formation of strong oxidizing reactive hydroxyl radical (•OH) generated from H_2O_2 can directly participate in the MB dye degradation reaction (Eq. 7,9) (Thulasi Karunakaran et al. 2022). Additionally, H_2O_2 can suppress e^-/h^+ pair recombination by acting as e^- acceptor and producing both hydroxide ions (OH^-) and hydroxyl radicals (Eq. 8). These OH^- react with holes (h^+) and decrease the rate of e^-/h^+ pair recombination, which contributes to the increased photodegradation of MB in the presence of H_2O_2 (Eq. 5, 9). However, increasing the MB concentration from 11.75 to 83 mg L^{-1} causes an increase in the turbidity of the solution, making it difficult for the visible light source to penetrate the solution, resulting in reduced degradation efficiency accordingly (Saha et al. 2018).

$$\mathrm{NH_2-MOF-5/MCOF} + h\nu \rightarrow \mathrm{e^-} + \mathrm{h^+} \quad (4)$$

$$\mathrm{h^+ + OH^- \rightarrow \cdot OH} \quad (5)$$

$$\mathrm{e^- + O_2 \rightarrow O_2^-} \quad (6)$$

$$\mathrm{H_2O_2 \rightarrow 2 \cdot OH} \quad (7)$$

$$\mathrm{e^- + H_2O_2 \rightarrow \cdot OH + OH^-} \quad (8)$$

$$\mathrm{MB + \left(O_2^- \cdot + h^+ + \cdot OH\right) \rightarrow CO_2 + H_2O + byproducts} \quad (9)$$

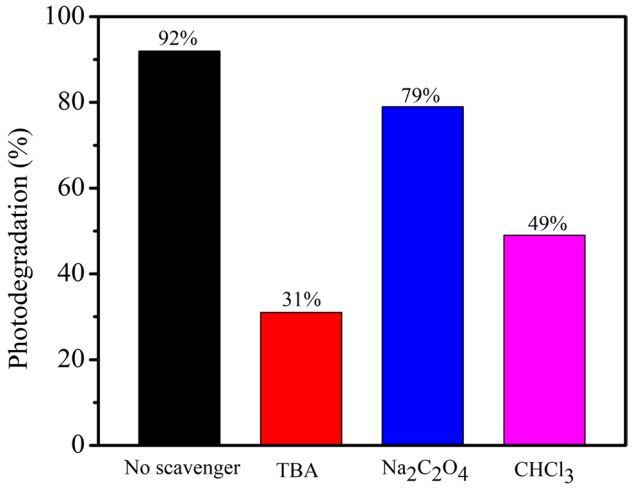

Fig. 10 Scavenger experiments for the MB photodegradation ([MB] = 30 mg L^{-1}, MB volume = 25 mL, pH = 9.5, NH_2-MOF-5/MCOF = 60 mg, $[H_2O_2] = 0.06$ mol L^{-1}, light source–5 W LED, 400–700 nm, $[TBA] = [Na_2C_2O_4] = [CHCl_3] = 1$ mM)

Scavenger test

In order to understand the contribution of different species present in the MB degradation, scavenger test was performed. Scavengers are compounds utilized to selectively quench specific reactive oxygen species (ROS) or radicals generated during chemical reactions. In this study, the scavengers TBA (tert-butyl alcohol), $Na_2C_2O_4$ (sodium oxalate), and $CHCl_3$ (chloroform) were employed for the purpose of quenching ·OH,h^+ and O_2^-· respectfully. According to Fig. 10, the degradation percentages of MB vary significantly when employing different scavengers. When no scavenger was used, the degradation of MB reached 92%, indicating the effectiveness of the photocatalytic process in the absence of scavenger. However, when scavengers were introduced, TBA resulted in only 31% degradation, $CHCl_3$ led to 49%, and $Na_2C_2O_4$ exhibited the highest degradation percentage at 79% which shows that all three species (·OH, O_2^-· and h^+) contribute to the photocatalytic degradation of MB and ·OH is the main species responsible for the photocatalytic degradation.

Reusability and stability of the hybrid catalyst

In order to assess the reusability and stability of the NH_2-MOF-5/MCOF material, recycling experiments were conducted as illustrated in Fig. 11a–c. Specifically, the resultant solution was filtered and washed with ethanol after each photocatalytic experiment, and the dried catalyst was subsequently reused. Remarkably, our catalyst exhibits a distinct characteristic of increasing photocatalytic activity from 92 to 100% for up to three cycles and maintains a high catalytic efficiency for up to six cycles (Fig. 11a, b). This exceptional behavior can be attributed to surface modification of the catalyst material resulting from longer visible

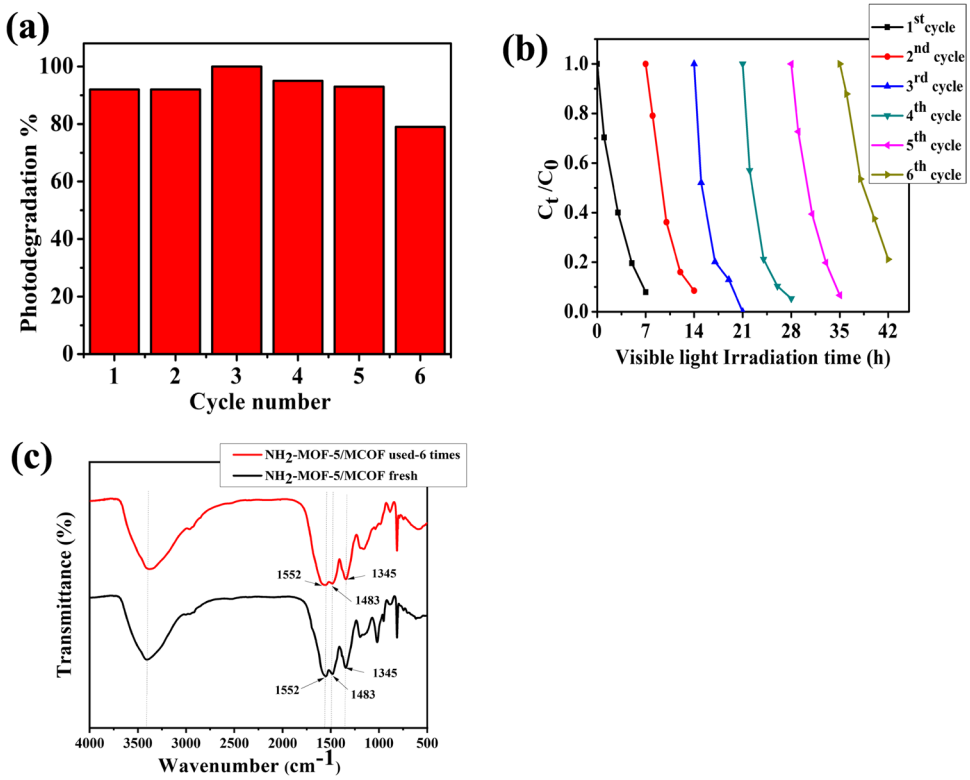

Fig. 11 **a** Photodegradation efficiency with respect to cycle number. **b** Concentration ratio of the material with respect to the visible light irradiation time. **c** FT-IR spectra of fresh NH_2-MOF-5/MCOF and after six times used NH_2-MOF-5/MCOF (condition—30 mg L^{-1} MB volume = 25 mL, catalyst weight 60 mg, light source—5 W LED (400–700 nm))

light exposure, which induces greater passivation of the catalyst nanoparticles (Dan et al. 2011; Kaur et al. 2014). Consequently, the hole–electron recombination rate is lowered, leading to the increasing of photodegradation efficiency. Nevertheless, after three cycles, the photodegradation efficiency may decrease due to catalyst loss occurring during washing and filtration in each cycle (Ranjith and Rajendra Kumar 2017; Thulasi Karunakaran et al. 2022). Figure 11c shows the FTIR analysis for both the fresh catalyst and the catalyst after six cycles of use. The analysis revealed that the FT-IR spectra of the catalyst remained unchanged, with the peak positions remaining the same. However, there was a slight decrease in the intensity of the peaks after multiple cycles of use. This observation highlights the remarkable stability of the NH_2-MOF-5/MCOF material, indicating that it retains its structural integrity and key functional groups even after prolonged use. Overall, our findings highlight the remarkable reusability and stability of the NH_2-MOF-5/MCOF material, which could pave the way for its application in large-scale wastewater treatment.

Conclusions

In summary, this study presents the synthesis and characterization of a highly efficient and environmentally friendly H_2O_2-assisted NH_2-MOF-5/MCOF hybrid material using a solvothermal method. SEM analysis revealed well-dispersed MCOF material onto the NH_2-MOF-5 surface, while XRD patterns showed a broad peak indicating the successful retention of MCOF, with less intense NH_2-MOF-5 peaks confirming the formation of the NH_2-MOF-5/MCOF hybrid. FT-IR spectra supported these findings, indicating the formation of C = N, C = C, and C-N bonds matching literature. UV-DRS data indicated efficient absorption of low-power visible light, facilitating the photodegradation process with a very low band gap of 2.20 eV. The remarkable efficacy of the H_2O_2-assisted NH_2-MOF-5/MCOF hybrid material in methylene blue photodegradation was demonstrated, achieving a 92% removal of 30 mg L^{-1} MB within 7 h, with a notable 3.5-fold increase in the degradation rate compared to the material without H_2O_2. Furthermore, it exhibits outstanding reusability, maintaining high catalytic efficiency for up to six cycles, and remarkable stability without altering its original structure over the same six cycles. We proposed a heterojunction formed between NH_2-MOF-5 and MCOF, suppressing e^-/h^+ pair recombination and enhancing electron transport rate, with •OH identified as the major species alongside $O_2^-\cdot$ and h^+, also responsible for MB photodegradation. Moreover, the H_2O_2-assisted hybrid material efficiently removed 99% of ibuprofen from aqueous solutions in just 12 min, suggesting its potential applicability in the removal of various organic pollutants.

Supplementary Information The online version contains supplementary material available at https://doi.org/10.1007/s11356-024-34552-8.

Author contribution Yen-Ping Peng and Po-Jung Huang: supervision, writing, and review. Amila Kasun Abeysinghe: material preparation, data collection, and analysis. The first draft of the manuscript was written by Amila Kasun Abeysinghe. Chia-Hung Chen, Wu-Xing Chen, Fang-Yu Liang, and Po-Yen Chien: writing, review, and editing. Yen-Ping Peng, Po-Jung Huang, and Ku-Fan Chen: conceptualization. Yen-Ping Peng and Po-Jung Huang: final revision. All authors read and approved the final manuscript.

Funding This work was supported by the National Science and Technology Council under Project NSTC 110–2221-E-110–024 and 111–2221-E-008–111-MY3.

Data availability Data will be made available on reasonable request.

Declarations

Ethical approval Not applicable.

Consent to participate All the authors agreed to participate in this work.

Consent for publication All the authors agreed to publish this work in Environmental Science and Pollution Research.

Competing interests The authors declare no competing interests.

References

Alkaykh S, Mbarek A, Ali-Shattle EE (2020) Photocatalytic degradation of methylene blue dye in aqueous solution by MnTiO(3) nanoparticles under sunlight irradiation. Heliyon 6:e03663. https://doi.org/10.1016/j.heliyon.2020.e03663

Al-Tohamy R, Ali SS, Li F, Okasha KM, Mahmoud YAG, Elsamahy T, Jiao H, Fu Y, Sun J (2022) A critical review on the treatment of dye-containing wastewater: ecotoxicological and health concerns of textile dyes and possible remediation approaches for environmental safety. Ecotoxicol Environ Saf 231:https://doi.org/10.1016/j.ecoenv.2021.113160

Bibi R, Shen Q, Wei L, Hao D, Li N, Zhou J (2018) Hybrid BiOBr/UiO-66-NH(2) composite with enhanced visible-light driven photocatalytic activity toward RhB dye degradation. RSC Adv 8:2048–2058. https://doi.org/10.1039/c7ra11500h

Cai M, Qin L, You L, Yao Y, Wu H, Zhang Z, Zhang L, Yin X, Ni J (2020) Functionalization of MOF-5 with mono-substituents: effects on drug delivery behavior. RSC Adv 10:36862–36872. https://doi.org/10.1039/d0ra06106a

Chen G, Luo J, Cai M, Qin L, Wang Y, Gao L, Huang P, Yu Y, Ding Y, Dong X, Yin X, Ni J (2019) Investigation of metal-organic framework-5 (MOF-5) as an antitumor drug oridonin sustained release carrier. Molecules 24. https://doi.org/10.3390/molecules24183369

Dan Y, Seo K, Takei K, Meza JH, Javey A, Crozier KB (2011) Dramatic reduction of surface recombination by in situ surface passivation of silicon nanowires. Nano Lett 11:2527–2532. https://doi.org/10.1021/nl201179n

Fiaz M, Hussain D, Athar M (2021) Synthesis of transition metal oxide incorporated MOF-5 and NH2-MOF-5 as efficient photoanode for oxygen evolution reaction. Ionics 27:759–770. https://doi.org/10.1007/s11581-020-03866-1

Firoozi M, Rafiee Z, Dashtian K (2020) New MOF/COF hybrid as a robust adsorbent for simultaneous removal of auramine O and rhodamine B dyes. ACS Omega 5:9420–9428. https://doi.org/10.1021/acsomega.0c00539

Fito J, Abewaa M, Mengistu A, Angassa K, Ambaye AD, Moyo W, Nkambule T (2023) Adsorption of methylene blue from textile industrial wastewater using activated carbon developed from Rumex abyssinicus plant. Sci Rep 13:5427. https://doi.org/10.1038/s41598-023-32341-w

Foulady-Dehaghi R, Sohrabnezhad S (2021) Hybridization of Schiff base network and amino functionalized Cu based MOF to enhance photocatalytic performance. J Solid State Chem 303:122549. https://doi.org/10.1016/j.jssc.2021.122549

Gadipelli S, Guo Z (2014) Postsynthesis annealing of MOF-5 remarkably enhances the framework structural stability and CO2 uptake. Chem Mater 26:6333–6338. https://doi.org/10.1021/cm502399q

Gao J, Huang Q, Wu Y, Lan Y-Q, Chen B (2021) Metal–organic frameworks for photo/electrocatalysis. Adv Energy Sustain Res 2. https://doi.org/10.1002/aesr.202100033

Ghosh S, Nakada A, Springer MA, Kawaguchi T, Suzuki K, Kaji H, Baburin I, Kuc A, Heine T, Suzuki H, Abe R, Seki S (2020) Identification of prime factors to maximize the photocatalytic hydrogen evolution of covalent organic frameworks. J Am Chem Soc 142:9752–9762. https://doi.org/10.1021/jacs.0c02633

Guo J, Ma J-F, Li J-J, Yang J, Xing S-X (2012) Unusual 2D → 3D polycatenane frameworks based on 1D → 2D interdigitated layers: from single crystals to submicrometer fibers with enhanced UV photocatalytic degradation performances. Cryst Growth Des 12:6074–6082. https://doi.org/10.1021/cg301208d

Gupta NK, Bae J, Kim S, Kim KS (2021) Terephthalate and trimesate metal-organic frameworks of Mn Co, and Ni: exploring photostability by spectroscopy. RSC Adv 11:8951–8962. https://doi.org/10.1039/d1ra00181g

Hadjiivanov KI, Panayotov DA, Mihaylov MY, Ivanova EZ, Chakarova KK, Andonova SM, Drenchev NL (2021) Power of infrared and raman spectroscopies to characterize metal-organic frameworks and investigate their interaction with guest molecules. Chem Rev 121:1286–1424. https://doi.org/10.1021/acs.chemrev.0c00487

Hafizovic J, Bjørgen M, Olsbye U, Dietzel PDC, Bordiga S, Prestipino C, Lamberti C, Lillerud KP (2007) The inconsistency in adsorption properties and powder XRD data of MOF-5 is rationalized by framework interpenetration and the presence of organic and inorganic species in the nanocavities. J Am Chem Soc 129:3612–3620. https://doi.org/10.1021/ja0675447

He S, Rong Q, Niu H, Cai Y (2019) Platform for molecular-material dual regulation: a direct Z-scheme MOF/COF heterojunction with enhanced visible-light photocatalytic activity. Appl Catal B 247:49–56. https://doi.org/10.1016/j.apcatb.2019.01.078

Holder CF, Schaak RE (2019) Tutorial on Powder X-ray Diffraction for Characterizing Nanoscale Materials. ACS Nano 13:7359–7365. https://doi.org/10.1021/acsnano.9b05157

Huang D, Yan X, Yan M, Zeng G, Zhou C, Wan J, Cheng M, Xue W (2018a) Graphitic carbon nitride-based heterojunction photoactive nanocomposites: applications and mechanism insight. 10:21035–21055. ACS Appl Mater Interfaces 10:21035–21055. https://doi.org/10.1021/acsami.8b03620

Huang X, Wu Z, Zheng H, Dong W, Wang G (2018b) A sustainable method toward melamine-based conjugated polymer semiconductors for efficient photocatalytic hydrogen production under visible light. Green Chem 20:664–670. https://doi.org/10.1039/c7gc02231j

Islam SMKN, Kurny ASW, Gulshan F (2015) Degradation of Commercial Dyes Using Mill Scale by photo-Fenton. Environ Processes 2:215–224. https://doi.org/10.1007/s40710-014-0055-1

Jawad AH, Mubarak NSA, Ishak MAM, Ismail K, Nawawi WI (2018) Kinetics of photocatalytic decolourization of cationic dye using porous TiO2 film. J Taibah Univ Sci 10:352–362. https://doi.org/10.1016/j.jtusci.2015.03.007

Ji W-J, Zhai Q-G, Li S-N, Jiang Y-C, Hu M-C (2012) The ionothermal synthesis of a 3D indium metal–organic framework: crystal structure, photoluminescence property and photocatalytic activity. Inorg Chem Commun 24:209–211. https://doi.org/10.1016/j.inoche.2012.07.014

Jing C, Zhang Y, Zheng J, Ge S, Lin J, Pan D, Naik N, Guo Z (2022) In-situ constructing visible light CdS/Cd-MOF photocatalyst with enhanced photodegradation of methylene blue. Particuology 69:111–122. https://doi.org/10.1016/j.partic.2021.11.013

Kalanur SS (2019) Structural, optical, band edge and enhanced photoelectrochemical water splitting properties of tin-doped WO3. Catalysts 9:456. https://doi.org/10.3390/catal9050456

Kaur J, Sharma M, Pandey OP (2014) Synthesis, characterization, photocatalytic and reusability studies of capped ZnS nanoparticles. Bull Mater Sci 37:931–940. https://doi.org/10.1007/s12034-014-0028-z

Kayan GO, Kayan A (2021) Inorganic–organic hybrid materials of zirconium and aluminum and their usage in the removal of methylene blue. J Inorg Organomet Polym Mater 31:3613–3623. https://doi.org/10.1007/s10904-021-01961-y

Keerthana S, Rani BJ, Yuvakkumar R, Ravi G, Saravanakumar B, Pannipara M, Al-Sehemi AG, Velauthapillai D (2021) NiMoO4 nanorods photocatalytic activity comparison under UV and visible light. Environ Res 197:111073. https://doi.org/10.1016/j.envres.2021.111073

Khan I, Saeed K, Zekker I, Zhang B, Hendi AH, Ahmad A, Ahmad S, Zada N, Ahmad H, Shah LA, Shah T, Khan I (2022) Review on methylene blue: its properties, uses, toxicity and photodegradation. Water 14. https://doi.org/10.3390/w14020242

Krishnaraj C, Sekhar Jena H, Bourda L, Laemont A, Pachfule P, Roeser J, Chandran CV, Borgmans S, Rogge SMJ, Leus K, Stevens CV, Martens JA, Van Speybroeck V, Breynaert E, Thomas A, Van Der Voort P (2020) Strongly reducing (diarylamino) benzene-based covalent organic framework for metal-free visible light photocatalytic H2O2 generation. J Am Chem Soc 142:20107–20116. https://doi.org/10.1021/jacs.0c09684

Kumari H, Sonia S, Ranga R, Chahal S, Devi S, Sharma S, Kumar S, Kumar P, Kumar S, Kumar A, Parmar R (2023) A review on photocatalysis used for wastewater treatment: dye degradation. Water Air Soil Pollut 234:349. https://doi.org/10.1007/s11270-023-06359-9

Li X, Pi Y, Wu L, Xia Q, Wu J, Li Z, Xiao J (2017) Facilitation of the visible light-induced Fenton-like excitation of H2O2 via heterojunction of g-C3N4/NH2-iron terephthalate metal-organic framework for MB degradation. Appl Catal B 202:653–663. https://doi.org/10.1016/j.apcatb.2016.09.073

Li F, Wang D, Xing Q-J, Zhou G, Liu S-S, Li Y, Zheng L-L, Ye P, Zou J-P (2019) Design and syntheses of MOF/COF hybrid materials via postsynthetic covalent modification: an efficient strategy to boost the visible-light-driven photocatalytic performance. Appl Catal B 243:621–628. https://doi.org/10.1016/j.apcatb.2018.10.043

Liu Y, Yu L, Hu Y, Guo C, Zhang F, Wen David Lou X (2012) A magnetically separable photocatalyst based on nest-like gamma-Fe(2)O(3)/ZnO double-shelled hollow structures with enhanced photocatalytic activity. Nanoscale 4:183–187. https://doi.org/10.1039/c1nr11114k

Liu J, Yuan J, Luo X, Hu H, Yang Z, Sun Q, Hou X, Xu D (2023) Constructing novel inorganic-organic α-Fe2O3/SNW-1 Z-scheme heterojunction for methylene blue photodegradation. J Solid State Chem 327:124242. https://doi.org/10.1016/j.jssc.2023.124242

Ma S, Xia X, Song Q, Zhao Y, Yang J (2023) Heterogeneous junction Ni-MOF@BiOBr composites: photocatalytic degradation of

methylene blue and ciprofloxacin. Solid State Sci 138:107135. https://doi.org/10.1016/j.solidstatesciences.2023.107135
Makuła P, Pacia M, Macyk W (2018) How to correctly determine the band gap energy of modified semiconductor photocatalysts based on UV–vis spectra. J Phys Chem Lett 9:6814–6817. https://doi.org/10.1021/acs.jpclett.8b02892
Marban G, Vu TT, Valdes-Solis T (2011) A simple visible spectrum deconvolution technique to prevent the artefact induced by the hypsochromic shift from masking the concentration of methylene blue in photodegradation experiments. Appl Catal A 402:218–223. https://doi.org/10.1016/j.apcata.2011.06.009
Matalkeh M, Nasrallah GK, Shurrab FM, Al-Absi ES, Mohammed W, Elzatahry A, Saoud KM (2022) Visible light photocatalytic activity of Ag/WO3 nanoparticles and its antibacterial activity under ambient light and in the dark. Results Eng 13:100313. https://doi.org/10.1016/j.rineng.2021.100313
Muller M, Turner S, Lebedev OI, Wang Y, van Tendeloo G, Fischer RA (2011) Au@MOF-5 and Au/MOx@MOF-5 (M = Zn, Ti;x= 1, 2): preparation and microstructural characterisation. Eur J Inorg Chem 2011:1876–1887. https://doi.org/10.1002/ejic.201001297
Oladoye PO, Ajiboye TO, Omotola EO, Oyewola OJ (2022) Methylene blue dye: toxicity and potential elimination technology from wastewater. Results Eng 16:100678. https://doi.org/10.1016/j.rineng.2022.100678
Peng MM, Jeon UJ, Ganesh M, Aziz A, Vinodh R, Palanichamy M, Jang HT (2014) Oxidation of ethylbenzene using nickel oxide supported metal organic framework catalyst. Bull Korean Chem Soc 35:3213–3218. https://doi.org/10.5012/bkcs.2014.35.11.3213
Peng H, Raya J, Richard F, Baaziz W, Ersen O, Ciesielski A, Samori P (2020) Synthesis of robust MOFs@COFs porous hybrid materials via an aza-Diels-Alder reaction: towards high-performance supercapacitor materials. Angew Chem Int Ed 59:19602–19609. https://doi.org/10.1002/anie.202008408
Periyasamy S, Viswanathan N (2019) Hydrothermal synthesis of melamine-functionalized covalent organic polymer-blended alginate beads for iron removal from water. J Chem Eng Data 64:2280–2291. https://doi.org/10.1021/acs.jced.8b01085
Qian LL, Wang ZX, Zhu LM, Li K, Li BL, Wu B (2019) Synthesis, structure, spectral characteristic and photocatalytic degradation of organic dyes of a copper metal-organic framework based on tri(triazole) and pimelate. Spectrochim Acta Part A 214:372–377. https://doi.org/10.1016/j.saa.2019.02.059
Quang TT, Truong NX, Minh TH, Tue NN, Ly GTP (2020) Enhanced photocatalytic degradation of MB under visible light using the modified MIL-53(Fe). Top Catal 63:1227–1239. https://doi.org/10.1007/s11244-020-01364-2
Rafatullah M, Sulaiman O, Hashim R, Ahmad A (2010) Adsorption of methylene blue on low-cost adsorbents: a review. J Hazard Mater 177:70–80. https://doi.org/10.1016/j.jhazmat.2009.12.047
Rajan A, Yazhini C, Dhileepan MD, Neppolian B (2024) Leveraging the photocatalytic Cr (VI) reduction by an IRMOF-3@NH2-MIL-101 (Fe) heterostructure based on interfacial Lewis acid-base interaction. Chemosphere 352:141473. https://doi.org/10.1016/j.chemosphere.2024.141473
Ranjith KS, Rajendra Kumar RT (2017) Regeneration of an efficient, solar active hierarchical ZnO flower photocatalyst for repeatable usage: controlled desorption of poisoned species from active catalytic sites. RSC Adv 7:4983–4992. https://doi.org/10.1039/c6ra27380g
Rapo E, Tonk S (2021) Factors affecting synthetic dye adsorption; desorption studies: a review of results from the last five years (2017–2021). Molecules 26. https://doi.org/10.3390/molecules26175419
Ren Q, Wei F, Chen H, Chen D, Ding B (2021) Preparation of Zn-MOFs by microwave-assisted ball milling for removal of tetracycline hydrochloride and Congo red from wastewater. Green Process Synth 10:125–133. https://doi.org/10.1515/gps-2021-0020
Reza KM, Kurny ASW, Gulshan F (2015) Parameters affecting the photocatalytic degradation of dyes using TiO2: a review. Appl Water Sci 7:1569–1578. https://doi.org/10.1007/s13201-015-0367-y
Saha D, Desipio MM, Hoinkis TJ, Smeltz EJ, Thorpe R, Hensley DK, Fischer-Drowos SG, Chen J (2018) Influence of hydrogen peroxide in enhancing photocatalytic activity of carbon nitride under visible light: an insight into reaction intermediates. J Environ Chem Eng 6:4927–4936. https://doi.org/10.1016/j.jece.2018.07.030
Senthilkumaar S, Varadarajan PR, Porkodi K, Subbhuraam CV (2005) Adsorption of methylene blue onto jute fiber carbon: kinetics and equilibrium studies. J Colloid Interface Sci 284:78–82. https://doi.org/10.1016/j.jcis.2004.09.027
Shan C, Zhang X, Ma S, Xia X, Shi Y, Yang J (2022) Preparation and application of bimetallic mixed ligand MOF photocatalytic materials. Colloids Surf A 636:128108. https://doi.org/10.1016/j.colsurfa.2021.128108
Slama HB, Chenari Bouket A, Pourhassan Z, Alenezi FN, Silini A, Cherif-Silini H, Oszako T, Luptakova L, Golińska P, Belbahri L (2021) Diversity of synthetic dyes from textile industries, discharge impacts and treatment methods. Appl Sci 11:6255. https://doi.org/10.3390/app11146255
Tellez SCA, Hollauer E, Mondragon MA, Castaño VM (2001) Fourier transform infrared and Raman spectra, vibrational assignment and ab initio calculations of terephthalic acid and related compounds. Spectrochim Acta Part A 57:993–1007. https://doi.org/10.1016/S1386-1425(00)00428-5
Thulasi Karunakaran S, Pavithran R, Sajeev M, Mohan Mohan Rema S (2022) Photocatalytic degradation of methylene blue using a manganese based metal organic framework. Results Chem 4:100504. https://doi.org/10.1016/j.rechem.2022.100504
Wan Y, Yang H, Shang Q, Cheng Q, Zhou H, Pan Z (2022) Integrating hollow spherical covalent organic frameworks on NH2–MIL-101(Fe) as high performance heterogeneous photocatalysts. Environ Sci Nano 9:3081–3093. https://doi.org/10.1039/D2EN00393G
Wang M, Guo L, Cao D (2018) Amino-functionalized luminescent metal–organic framework test paper for rapid and selective sensing of SO2 gas and its derivatives by luminescence turn-on effect. Anal Chem 90:3608–3614. https://doi.org/10.1021/acs.analchem.8b00146
Wang Q, Gao Q, Al-Enizi AM, Nafady A, Ma S (2020) Recent advances in MOF-based photocatalysis: environmental remediation under visible light. Inorg Chem Front 7:300–339. https://doi.org/10.1039/c9qi01120j
Wen Q, Sun T, Wang Q, Huang W, Liu Y (2019) Unique thiophilic affinity MOFs as specific sorbent for disulfide bond-containing compounds capture. SN Appl Sci 1. https://doi.org/10.1007/s42452-019-0799-3
Wu H, Tan HL, Toe CY, Scott J, Wang L, Amal R, Ng YHJAM (2020) Photocatalytic and photoelectrochemical systems: similarities and differences. Adv Mater 32:e1904717. https://doi.org/10.1002/adma.201904717
Yan X, Xu T, Chen G, Yang S, Liu H, Xue Q (2004) Preparation and characterization of electrochemically deposited carbon nitride films on silicon substrate. J Phys D Appl Phys 37:907–913. https://doi.org/10.1088/0022-3727/37/6/015
Yan X, Zhao Y, Du G, Guo Q, Chen H, He Q, Zhao Q, Ye H, Wang J, Yuan Y, Yue T (2022) Magnetic capture of sulfur quantum dots encapsulated in MOF-5-NH2 via a target-driven self-cycling catalyzed hairpin assembly for the sensitive detection of patulin. Chem Eng J 433. https://doi.org/10.1016/j.cej.2021.133624
Yang L-M, Fang G-Y, Ma J, Ganz E, Han SS (2014) Band gap engineering of paradigm MOF-5. Cryst Growth Des 14:2532–2541. https://doi.org/10.1021/cg500243s

Younas M, Rezakazemi M, Daud M, Wazir MB, Ahmad S, Ullah N, Inamuddin RS (2020) Recent progress and remaining challenges in post-combustion CO2 capture using metal-organic frameworks (MOFs). Prog Energy Combust Sci 80:100849. https://doi.org/10.1016/j.pecs.2020.100849

Zhang Y, Liu H, Gao F, Tan X, Cai Y, Hu B, Huang Q, Fang M, Wang X (2022) Application of MOFs and COFs for photocatalysis in CO2 reduction, H2 generation, and environmental treatment. EnergyChem 4. https://doi.org/10.1016/j.enchem.2022.100078

Zhou S, Kong Z-G, Wang Q-W, Li C-B (2012) Synthesis, structure and photocatalytic property of a novel 3D (3,8)-connected metal–organic framework based on a flexible triphosphonate and a pentanuclear Cu(II) unit. Inorg Chem Commun 25:1–4. https://doi.org/10.1016/j.inoche.2012.08.015